Current Chemistry Letters 12 (2023) 55–64

Contents lists available atGrowingScience

Current Chemistry Letters

homepage: www.GrowingScience.com

Synthesis, spectroscopic characterization and biological activities of some metal complexes with new heterocyclic azodye ligand 2-(2-hydroxynaphthalen-1-yl azo)-pyridin-3-ol

V. G. Vidya[a*] and V. Sadasivan[a]

[a]*Department of Chemistry, University College, M. G. Road, Trivandrum-69503, Kerala, India*

C H R O N I C L E

Article history:
Received March 21, 2022
Received in revised form
April 20, 2022
Accepted September 28, 2022
Available online
September 28, 2022

Keywords:
2-amino-3-hydroxypyridine
β-naphthol
Azodye
DNA cleavage
Biological activity

A B S T R A C T

Metal complexes of [2-(2-hydroxynaphthalen-1-ylazo)-pyridin-3-ol] are derived from 2-amino-3-hydroxypyridine and *β*-naphthol was synthesized and characterized by thermal, spectral and analytical tools. The ligand was reacted with Mn(II), Fe(II), Co(II), Ni(II), Cu(II) and Zn(II) in 1:2 stoichiometry. The IR spectra confirms the azo ligand coordination to metal ions via azo nitrogen and phenolic oxygen of pyridine after deprotonation. Both IR and ^{1}HNMR spectra recorded involvement of deprotonated hydroxyl groups with proton displacement. The magnified fluorescence was shown by Mn(II) and Ni(II) complexes. None of the prepared ligands or complexes show any NLO activity with KDP as standard. The DNA cleavage and anticancerous activities done. The influence of zinc chelates on cure characteristics of rubber compounds was estimated based on rheometer measurements. The ligand and metal complexes are tested in vitro against some bacteria and fungi species. The antioxidant activities, DNA cleavage and anticancerous activities done. Ligand and its complexes catalysed cleavage of DNA.

1. Introduction

Azo dyes take the place of highly coloured compounds that are produced in large volume and its allied importance may increase in the future. More than 60% of total dyes accounts to azo dyes. Azo dyes are established as the most ingenious and significant category among organic compounds with various purposes in science and technology. The role in execution of dye of appropriate attribute colour, yield and grain size can be assembled by different routes and alterations. The role in execution of dye as synthetic colourants in textile,[1,2] printing[3,4] and in paper manufacturing is very significant.[5,6] Azo dyes are widely used in liquid crystal display colour filters,[7] lasers, nonlinear optics, photovoltaic production,[8] chemical sensors, as drug, cosmetics, food and in many organic synthesis[9]. Azo groups attached to benzene rings, naphthalenes, aromatic heterocycles or to enolizable groups give colour of different intensities. Synthesis and characterization of ligands has a major role in developing metal complexes. Due to electron donating, electron accepting, constitutional and functional groups, identity of ligand in coordination sphere complexes shows distinctive characteristics and novel receptiveness.[10] Azo dyes also act as corrosion inhibitors in recent times.[11,12] Metal azo dye complexes are used in dying leather.[13,14] Pyridine derivatives exhibit significant contribution in several biochemical reactions. Pyridine ring molecular systems having chelating molecular designs, have been examined in the field of mycology for developing metal-based drugs. In several years, endeavours have been made to implement and amplify drugs based on pyridine molecules.[15,16] There are a wide range of metal complexes of azo dyes containing pyridine, pyrimidine and imidazole groups that were used for DNA cleavage. Such azo complexes take part in significant contribution in biological and biomedical affairs and it is perceptible that many organic modes of deeds are operated or bio transformed by transition metal ions due to large number of coordination numbers and geometries.

* Corresponding author.
E-mail address vg_vidya@yahoo.co.in (V. G. Vidya)

doi: 10.5267/j.ccl.2022.9.006

In the present study, we aim to design and synthesize novel azo compounds and their Mn(II), Fe(II), Co(II), Ni(II), Cu(II) and Zn(II) complexes of [2-(2-hydroxynaphthalen-1-ylazo)-pyridin-3-ol] (BNAP) that are characterized by different physico-chemical methods. There is no doubt that applied sciences have a great chemical, biomedical, and industrial importance.

2. Experimental

All reagents were purchased from Merck. The ^{1}HNMR spectra of ligand and Zn(II) complex taken in DMSO on a 400MHz FTNMR using TMS as reference material. The ESI mass spectrum of ligand and Zn(II) complex recorded on FTMS mass spectrometer. FT-IR were recorded on a Perkin-Elmer spectrum 65 infrared spectrometer using KBr pellets in the region 400-4000cm^{-1}. The electronic absorption measurements were recorded on Perkin-Elmer Lambda 25 UV-Visible Spectrophotometer in the range 200-800nm. The conductance is determined at room temperature using Systronics direct conductivity meter. The magnetic susceptibility was recorded on Sherwood Scientific magnetic susceptibility balance. The Electron Spin Resonance (ESR) spectra of Cu(II) complex recorded on a Varian E-112 spectrometer using Tetracyanoethylene (TCNE) as reference. The cyclic voltammetry (CV) of Co(II) complex recorded on BAS CV-50W voltammetric analyser. As the three-electrode system, a glassy carbon electrode (3 mm diameter) was used as a working electrode, Ag/AgCl (3 M KCl) as a reference electrode, and platinum wire as auxiliary electrode. A 0.1 M H_2SO_4 solution supported the electrolyte, and DMF was used to dissolve all synthesized compounds. The electrochemical measurement was carried out in 10^{-3} M Co(II) complex. The recording was done in an inert atmosphere. The fluorescence spectra recorded on the JASCO-750 fluorescence spectrometer. The NLO activity was recorded from IISC Bangalore.

The ligand and complexes were subjected to antimicrobial study and screened against selected microbes, antioxidant activity by 2,2-diphenyl-1-picryl-hydrazyl-hydrate (DPPH) assay and cleavage efficiency compared to that of control. Co(II) complex evaluated for the anticancer studies against human cervical cancer cell line SiHa and human breast cell line $SkBr_3$.

2.1. Preparation of BNAP

The ligand [2-(2-hydroxynaphthalen-1-ylazo)-pyridin-3-ol] (BNAP) was prepared by standard procedure of diazotization.[17] 4.4g of 2-amino-3-hydroxypyridine dissolved in 50ml 1:1 HCl and kept at 0^{o}C. 1.4g sodium nitrite kept in ice cold was added slowly to the above solution with stirring. The resultant solution was permitted to stand in the ice bath for 30 minutes. 5g of β- naphthol was dissolved in 45ml 10% NaOH and cooled to 0^{o}C. Added to this, the above diazotized solution of 2-amino-3-hydroxypyridine with stirring. The resultant solution was allowed to stand for 30 minutes at room temperature. A dark grey substance was precipitated. filtered and washed with ethanol-water mixture. Dried over anhydrous $CaCl_2$. Yield was 80% and recrystallized from ethanol. The dyeing application of ligand and its fastness properties studied and reported.[18]

2.2. Preparation of complexes

The complexes of BNAP with Mn(II), Fe(II), Co(II), Ni(II), Cu(II) and Zn(II)complexes were prepared by the following general method.[14] A methanolic solution of the respective metal salt $Mn(Ac)_2.4H_2O$, $Co(NO_3)_2.6H_2O$, $NiCl_2.6H_2O$, $CuCl_2.2H_2O$ and $Zn(Ac)_2.2H_2O$ was added to a solution of BNAP in methanol in 1:1 ratio. The resulting mixture was stirred and refluxed for 3-4 hours. The solution is concentrated to get a solid complex. It was filtered, washed with ethanol, dried and kept in a desiccator over anhydrous $CaCl_2$.

3. Result and Discussions

The percentage of metal and chloride of the complexes were found using the standard methods.[19] Analytical data of complexes and ligands are given in Table1. From the elemental analyses complexes can have general molecular formula $[M(BNAP)_2(H_2O)_2]$ where M = Mn(II), Co(II), Ni(II), Cu(II) and Fe(II) and for Zn(II) is $[Zn(BNAP)_2]$.

Table 1. Analytical data of BNAP and its complexes

Compound	Mol Wt.	colour	M%		C%		H%		N%	
			Cal	Exp	Cal	Exp	Cal	Exp	Cal	Exp
BNAP	265	Grey	-	-	67.92	67.91	4.15	4.16	15.80	15.84
$[Mn(BNAP)_2(H_2O)_2]$	619	Black	8.87	8.86	58.16	58.15	3.55	3.56	13.57	13.59
$[Fe(BNAP)_2(H_2O)_2]$	622	Olive green	8.94	8.95	57.89	57.90	57.69	57.70	4.47	4.48
$[Co(BNAP)_2(H_2O)_2]$	625	Brown	10.00	10.03	57.78	57.75	3.53	3.71	13.48	13.50
$[Ni(BNAP)_2(H_2O)_2]$	624	Black	9.42	9.40	57.78	57.78	5.53	3.57	13.48	13.45
$[Cu(BNAP)_2(H_2O)_2]$	628	Black	10.11	10.08	57.32	57.39	3.50	3.58	13.37	13.31
$[Zn(BNAP)_2]$	593	Black	11.03	10.98	60.71	60.48	3.71	3.65	14.16	14.12

The proton NMR of BNAP gives a multiplet in range δ 7.07-7.71 ppm due to aryl protons.[19] The peak at δ 9.76 ppm is due to hydroxyl group on pyridine ring[19] and the other peak at δ 10.13 ppm may be due to hydroxyl group of *β*- naphthol part. The proton NMR of BNAP is shown in **Fig. 1.**

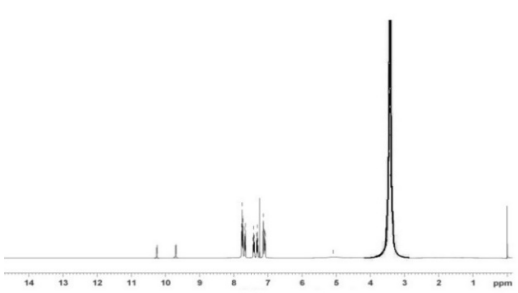

Fig. 1. [1]HNMRof BNAP

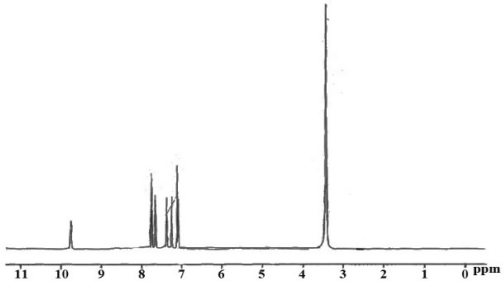

Fig. 2. [1]H NMR of $[Zn(BNAP)_2]$

The [1]HNMR spectrum of $[Zn(BNAP)_2]$ is given in **Fig. 2** shows three peaks, a multiplet between δ7.07-7.71 ppm (9H, m) due to aryl protons and a singlet at δ9.76 ppm (1H, s) is due to hydroxyl group on pyridine ring and another singlet at δ10.13 ppm (1H, s) due to hydroxyl group of *β*- naphthol. The multiplet observed at δ7.70 – 7.80ppm (9H, m), due to aryl proton in $[Zn(BNAP)_2]$, is shifted slightly towards the down field compared to BNAP. Among the two singlets at δ 9.76 and 10.13 ppm due to hydroxyl protons in BNAP, the latter is found absent and the former one underwent a shift to a lower field in its Zn(II) complex. This clearly expresses that the hydroxyl group on the naphthol ring alone gets deprotonated and coordinated to Zn(II) ion, while the other hydroxyl group remains unchanged.

The FTMS-ESI mass spectrum shows a peak of BNAP consisting of a peak corresponding to the species $[(C_{15}H_{11}N_3O_2)]^+$ at m/z 267 assignable to $[M + 2H]^+$ peak. The mass spectra of BNAP and $[Zn(BNAP)_2]$ is given in **Fig. 3**. and **Fig. 4**. The base peak corresponds to (M+ Na) at m/z 616, assignable to $[Zn(BNAP)_2Na]^+$. This mass spectral evidence substantiates the molecular formula $[Zn(BNAP)_2]$ obtained from elemental analysis. The mass spectra give proof for 1:2 metal ligand coordination. The IR spectra of the BNAP and complexes were recorded in the range 400 – 4000 cm^{-1}. The major bands and the tentative allocations are shown in **Table 2**. The -N=N- vibration of BNAP at 1468 cm^{-1} has shifted to 1427-1452 cm^{-1} in the IR spectra of complexes showing the involvement of azo group in coordination.[20] The band corresponds to hydrogen bonded hydroxyl group stretching appears at 3294 cm^{-1} in BNAP disappears in the IR spectra of all complexes. The other hydroxyl group absorption in BNAP spectrum at 3392 cm^{-1} remains intact in the spectrum of all complexes. This infers that out of two –OH, one gets coordinated after deprotonation and other remains free.[21] The new broad band appeared around 3412 cm^{-1}in IR spectra of complexes designates the existence of coordinated water molecules. The existence of coordinated water molecules is supported by the appearance of new bands in the ranges 1610-1600 and 970-950 cm^{-1} due to HOH deformation and rocking. The emergence of new band in region 510-523cm^{-1} due to ν_{M-O} supports the OH group coordination to metal ion after deprotonation and the bands in the range 415-435cm^{-1}due to ν_{M-N} supports -N=N- coordination to metal ion.[22] From IR spectra it is evident that BNAP is coordinated to metal ion in uninegative bidentate manner. The coordination sites of BNAP are the azo group and one of the hydroxyl groups after deprotonation.[23]

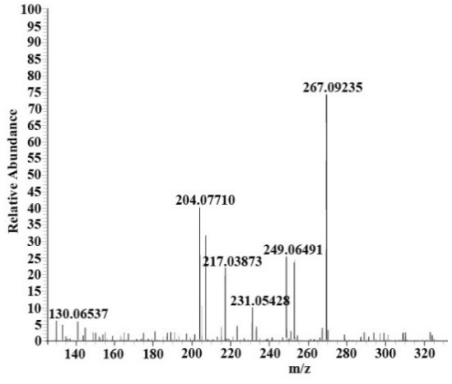

Fig. 3. Mass spectrum of BNAP

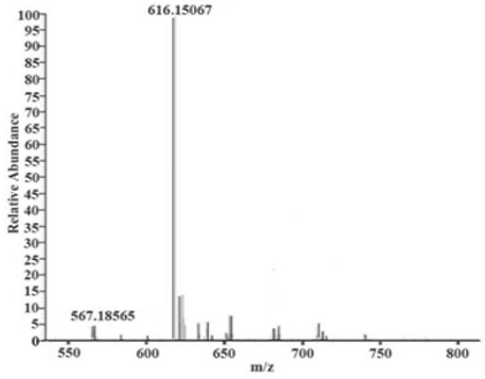

Fig. 4. Mass spectrum of $[Zn(BNAP)_2]$

The molar conductance values at room temperature were set on using 10^{-3}M solution of all the complexes in methanol and nitrobenzene and are presented in **Table 3**. From the molar conductance values the electrolytic nature of the complex, whether it is 1:1, 1:2, 1:3 or non-electrolyte can be found. The molar conductance value for all the BNAP complexes is of the order 2-17 Ω^{-1} cm^2 mol^{-1} in methanol and 1-11Ω^{-1} cm^2 mol^{-1} in nitrobenzene. The conductance values were compared with the data available for standards.[24] From the observed conductance values, it can be inferred that all complexes are non-

electrolytes. Magnetic values can provide information on the structure of the complexes and oxidation state of the central metal ion. The effective magnetic moment values of BNAP complexes are presented in Table3. Mn(II) complex of BNAP shows magnetic moment value 5.98 BM. This infers that the complex molecule $[Mn(BNAP)_2(H_2O)_2]$ is in high spin octahedral state[22]. The effective magnetic moment value calculated for Fe(II) is 4.26 BM for high spin octahedral complex.[21,25]

Table 2. Selected FTIR bands of BNAP and its complexes

BNAP	$[Mn(BNAP)_2(H_2O)_2]$	$[Fe(BNAP)_2(H_2O)_2]$	$[Co(BNAP)_2(H_2O)_2]$	$[Ni(BNAP)_2(H_2O)_2]$	$[Cu(BNAP)_2(H_2O)_2]$	$[Zn(BNAP)_2]$	Band assignments
3392 3294	3391 -	3392 -	3393 -	3391 -	3390 -	3391 -	ν_{OH}
-	3447	3225	3435	3379	3327	-	νH_2O
-	1610	1603	1609	1600	1602	-	$\nu_{HOH\ (def)}$
1468	1437	1448	1452	1439	1452	1443	$\nu_{N=N}$
-	950	970	969	965	963	-	$\nu_{HOH\ (rock)}$
-	518	530	527	525	507	529	ν_{M-O}
-	422	467	453	461	439	429	ν_{M-N}

The $[Fe(BNAP)_2(H_2O)_2]$ has octahedral geometry as evidenced from its magnetic moment data. The effective magnetic moment value calculated for the Co(II) complex of BNAP is 4.48 BM. This value agrees with high spin octahedral geometry of $[Co(BNAP)_2(H_2O)_2]$. The BNAP complex of Ni(II) shows a magnetic moment 2.93 BM.[26] This value suggests a high spin octahedral environment for $[Ni(BNAP)_2(H_2O)_2]$. The Cu(II) complex of BNAP shows a magnetic moment value of 2.08 BM which is in the range suggested for an octahedral complex. This observation suggests an octahedral geometry for $[Cu(BNAP)_2(H_2O)_2]$.[22]

Table 3. Molar conductance and magnetic moment values of BNAP complexes

Complex	Concentration x 10^{-3} M	Conductance (Ω^{-1} cm^2 mol^{-1})		Magnetic moment(BM)
		methanol	Nitrobenzene	
$[Mn(BNAP)_2(H_2O)_2]$	5.49	17	9	5.98
$[Fe(BNAP)_2(H_2O)_2]$	6.23	13	11	4.26
$[Co(BNAP)_2(H_2O)_2]$	5.88	8	3	4.48
$[Ni(BNAP)_2(H_2O)_2]$	6.24	9	7	2.93
$[Cu(BNAP)_2(H_2O)_2]$	6.35	2	1	2.08
$[Zn(BNAP)_2]$	5.95	6	5	Diamagnetic

The electronic spectral data helps us to arrive at results which was in accordance to magnetic susceptibility measurements. The Mn(II) complex of BNAP exhibits a very weak absorption at 525 nm because of conjoining of spin forbidden d-d transition to intense band at 404 nm due to n→π* intraligand absorption which suggests distorted octahedral geometry for the complex. Fe(II) complex exhibits three bands around 403 nm, 508 nm and 664 nm corresponds to n→π* intraligand transfer and $^5T_{2g} \rightarrow {}^5E_g$, that supports octahedral geometry for the complex. The $[Co(BNAP)_2(H_2O)_2]$ reveal peaks respectively at 398 nm, 565 nm and 622 nm corresponds to n→π* intraligand transfer, $^4T_{1g}(F) \rightarrow {}^4T_{1g}(P)$and $^4T_{1g}(F) \rightarrow {}^4A_{2g}(F)$ transformation proposes octahedral high spin geometry for Co(II).[26] The $[Ni(BNAP)_2(H_2O)_2]$ reveals absorptions at 403 nm, 482 nm and 552 nm corresponds ton→π* intraligand transfer, $^3A_{2g}(F) \rightarrow {}^3T_{1g}(P)$ and $^3A_{2g}(F) \rightarrow {}^3T_{1g}(F)$ transformation proposes an octahedral nature all over Ni(II).[27] The spectrum of newly synthesized Cu(II) exhibits a band at 409 nm corresponds to n→π* intraligand transfer and another very weak band at 518 nm which is caused by d – d transition. These transitions propose an octahedral geometry for the Cu(II) complex.[26]

The electronic abode of $[Cu(BNAP)_2(H_2O)_2]$ can be obtained from ESR spectra. The X band spectrum of $[Cu(BNAP)_2(H_2O)_2]$ taken at 300K in solution state gives an isotropic model because of tumbling motion of the molecules. Whereas the spectrum of the frozen solution at 77K exhibits anisotropic pattern with four distinct peaks in parallel range comparable to electron – nuclear spin interaction. The peak at 3200 G is typical of Cu(II) species. The absence of any half field absorption in range 1500-1600 G eliminates the possibility of metal-metal interaction in this complex. In $[Cu(BNAP)_2(H_2O)_2]$, observed g tensor values are $g_{\parallel}$ (2.43) >g $_{\perp}$ (2.07)>$g_e$free electron (2.0027) which recommends a distorted octahedral geometry and the system is axially symmetric.[28] The perpendicular part exhibits no hyperfine splitting and so $A_{\perp}$ is zero., The g – values in the axial spectrum are linked to the exchange interaction coupling constant G. The exchange interconnection is very less for G value is greater than four, because of parallel alignment of local tetragonal axes.[28] This Cu(II) complex of BNAP has G value 6.35 recommends misalignment of local tetragonal axes with ground state d_{x2-y2}. From the $\propto_{Cu}^{2}$value calculated for the complex is 0.99, shows covalent nature around the ligand.[28] The ESR spectrum of $[Cu(BNAP)_2(H_2O)_2]$ taken in frozen solution at 77K is shown in **Fig. 5**.

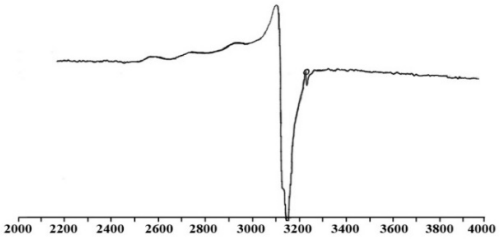

Fig. 5. ESR spectrum of $[Cu(BNAP)_2(H_2O)_2]$

The trend $g_{\parallel}$>g $_{\perp}$ >g_e2.0023 indicates the occupancy of odd electron in d_{x2-y2}orbital peculiarity of axial symmetry.[29,30] The g_{avg} calculated is 2.19. From these results $[Cu(BNAP)_2(H_2O)_2]$ possess distorted octahedral geometry. The CV of $[Co(BNAP)_2(H_2O)_2]$ is shown in **Figure 6**. CV of Co(II) displays two well defined quasi-reversible peaks.[31] The average of cathodic and anodic peak potentials average was taken and half wave potential for the reversible Co(III)/Co(II) and Co(II)/Co(I) redox couples calculated. Voltammogram exhibits a reduction peak at E_{pc} = - 0. 497 V and E_{pa} = - 0.682V. This couple can be reversed with ΔEp = 0.185 V. The anodic to cathodic peak currents ratio is ≈ 1 respective of one electron transfer process. The $[Co(BNAP)_2(H_2O)_2]$ exhibits a quasi-reversible oxidation peak, peculiar for Co(II)/Co(III) at E_{pc} = + 0.209 V and E_{pa} = + 0.327 V. The peak separation of this couple is 0.118 V. The reduction system has about a unit ratio of anodic to cathodic top currents (I_{pa}/I_{pc}). The ratio observed for oxidation procedure deviates from unity because of residual current at lesser potential. The results shown are because of one electrode process. The anodic-cathodic peak separation values of Co(III)/Co(II) and Co(II)/Co(I) couples are 52 and 58 mV respectively.[33] The value is anticipated for reversible one electron process.[32] The lesser value seen for the Co(III)/Co(II) and Co(II)/Co(I) couples shows the constancy of six coordination complex during the reduction processes. Upon reverse scan only the electron transfer processes take place and are not accompanied by chemical reaction. The Co(III) complexes reduce to Co(II) accompanying a chemical reaction as reported in literature. This is due to loss of an axial ligand due to addition of one electron to d_{z2} orbital. Here the reoxidation wave seemed at a high potential or upon reversal scan no corresponding anodic wave was observed.[33,34] Here axial ligands attached to central atom are not liberated on to the area of electrode during CV measurements and the reduction process has a reversible character.[35,36,37,38,39,40]

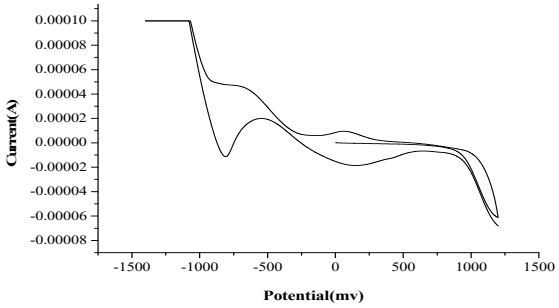

Fig. 6. CV of $[Co(BNAP)_2(H_2O)_2]$

The second harmonic generation performance of BNAP and its complexes had been determined. The performance of the sample was set side by side with microcrystalline powder of (potassium dihydrogen phosphate) KDP. Both ligands and complexes do not show NLO properties.

BNAP, $[Mn(BNAP)_2(H_2O)_2]$ and $[Ni(BNAP)_2(H_2O)_2]$ reveal fluorescence around 400-700 nm in methanol solution at room temperature. These transitions are allocated to intraligand ($\pi \rightarrow \pi^*$) fluorescence. The $[Mn(BNAP)_2(H_2O)_2]$ and

$[Ni(BNAP)_2(H_2O)_2]$ exhibit greater emission compared to free BNAP. Metal ions present in the complex magnifies the fluorescence. The fluorescence of BNAP, $[Mn(BNAP)_2(H_2O)_2]$ and $[Ni(BNAP)_2(H_2O)_2]$ are given in **Fig. 7**.

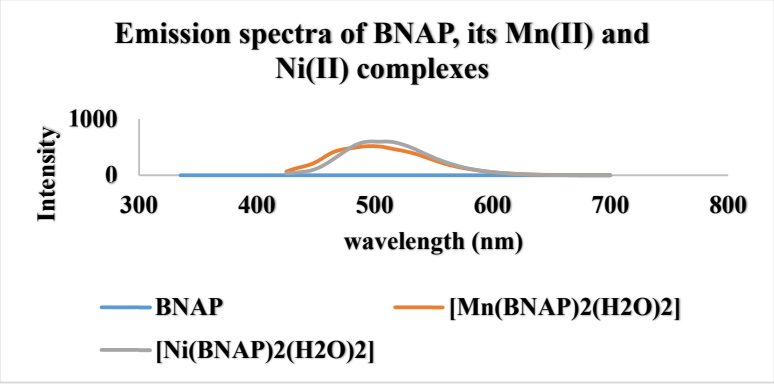

Fig. 7. Fluorescence spectra of BNAP, $[Mn(BNAP)_2(H_2O)_2]$ and $[Ni(BNAP)_2(H_2O)_2]$

BNAP on excitation at 410 nm shows an emission band at 550 nm. $[Mn(BNAP)_2(H_2O)_2]$ exhibits fluorescence at 503 nm and $[Ni(BNAP)_2(H_2O)_2]$ at 515 nm in excitation at 404 and 403 nm respectively. The emission peaks are enhanced up on coordination with Mn(II) and Ni(II). The photoluminescence data of BNAP, $[Mn(BNAP)_2(H_2O)_2]$ and $[Ni(BNAP)_2(H_2O)_2]$ are given in **Table 4**.

Table 4. Photoluminescence data of BNAP and its complexes

Compound	$\lambda_{excitation}$ (nm)	$\lambda_{emission}$ (nm)	Intensity of emission	Stokes shift
BNAP	410	550	0.80	140
$[Mn(BNAP)_2(H_2O)_2]$	404	503	514	99

The analytical data reveals metal to ligand ratio of BNAP complexes as 1:2. Molar conductance values suggest that these complexes are nonelectrolytes. The mass spectrum of $[Zn(BNAP)_2]$ concurs well with the exception. The presence of water is supported by the presence of a broad band around 3412 cm^{-1} in IR spectra. This can again be supported by the presence of additional bands in range 1610 – 1600 $cm^{-1}$and 970-950 cm^{-1} because of deformation and rocking of HOH. From the IR data of BNAP complexes it is indicative that BNAP is an uninegative bidentate ligand. The point of coordinations are azo nitrogen and phenolic oxygen on naphthol after deprotonation. The disappearance of hydroxyl proton of naphthol in ^{1}HNMR spectrum of $[Zn(BNAP)_2]$ supports this observation. The other peaks in NMR have gone to lower field showing the chelation of BNAP. The four coordinated Zn(II) complexes may have both tetrahedral and square planar geometry. However, most of the four coordinated zinc complexes exist in tetrahedral geometry. Therefore, we propose a tetrahedral structure for $[Zn(BNAP)_2]$. Magnetic and electronic spectral evidence says that all the complexes have octahedral geometry except for $[Zn(BNAP)_2]$, which shows tetrahedral geometry. This is supported by electronic spectra and magnetic moment values. Based on all evidence, the following structures are proposed for BNAP complexes, which are shown in **Fig. 8 and Fig. 9**.

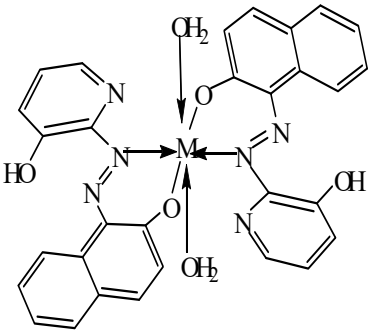

Fig. 8. Proposed structure of $[M(BNAP)_2(H2O)_2]$

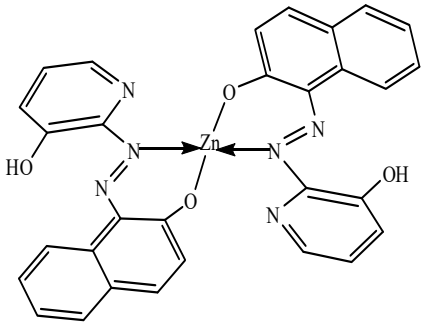

Fig. 9. proposed structure of $[Zn(BNAP)_2]$

Where M – Mn(II), Co(II), Ni(II), Cu(II), Fe(II)

BNAP is active for *Candida albicans* with respect to the standard, clotrimazole. Complexes also show activity but less compared to that of BNAP. The values of which are shown in **Table 5**. and in **Fig. 10 and Fig. 11**.

Table 5. Antimicrobial activity of BNAP and its complexes

Sample	Zone of inhibition in cm Volume of sample(µl)100			
	Bacteria		Fungi	
	S. aureus	*E. coli*	*A. niger*	*C. albicans*
Gentamycin	3.0	3.2	-	-
Clotrimazole	-	-	3.0	2.0
BNAP	3.0	3.0	1.2	2.6
$[Mn(BNAP)_2(H_2O)_2]$	1.7	1.6	1.0	1.9
$[Zn(BNAP)_2]$	2.5	2.3	1.4	2.1
$[Ni(BNAP)_2(H_2O)_2]$	2.0	2.1	1.3	2.0

BNAP exhibits comparable antioxidant activity to standard ascorbic acid, which decreases upon complexation and is represented in **Fig. 12**. On complexing BNAP with metals prevents oxyradical generation and consequent oxidative damage [41]. BNAP is showing an IC_{50} value of 20 ± 0.02 µg/ml, which is comparable to the ascorbic acid standard used. BNAP and its metal complexes are investigated against pUC 18 DNA by gel electrophoresis method for DNA cleavage activity. DNA cleavage studies are associated with redox active or photoactivated metal complexes. Due to this property transition metal complexes aid in DNA recognition [42,43]. BNAP and metal complexes as they have different molecular weight acts differently, between control and treated DNA, which can be clearly seen from electrophoresis analysis. This different behaviour can be seen in the band of lanes of complexes and BNAP because of relaxation of circular DNA to linear form and that can be compared to DNA pUC 18[44].

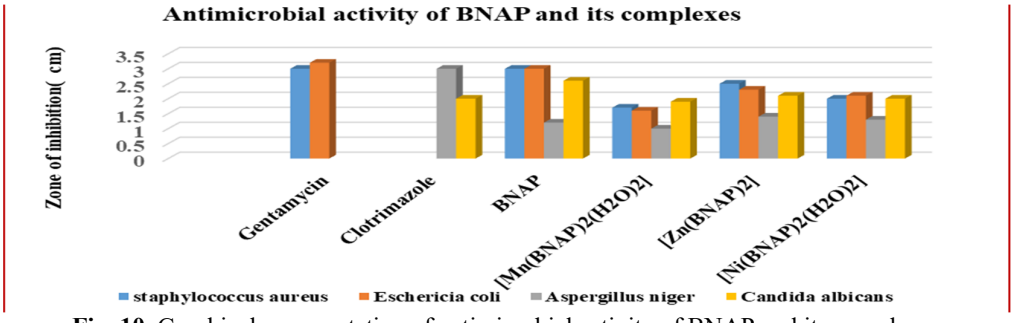

Fig. 10. Graphical representation of antimicrobial activity of BNAP and its complexes

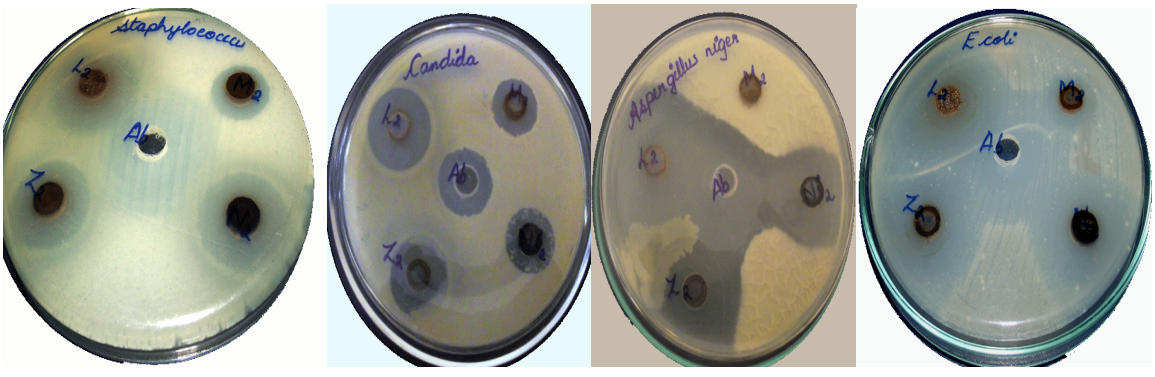

Fig. 11. Antimicrobial activity of BNAP and its complexes

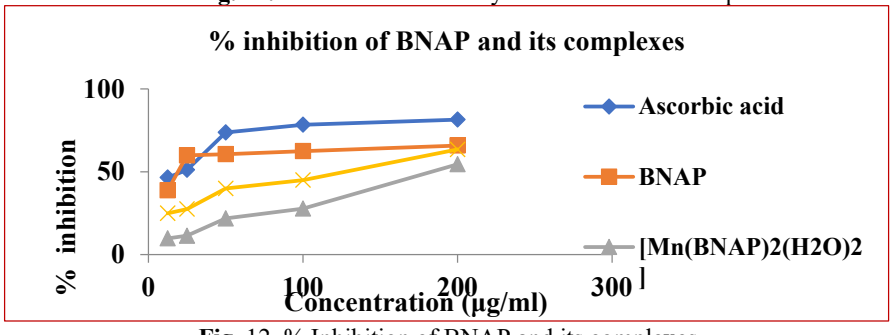

Fig. 12. % Inhibition of BNAP and its complexes

The results show that the control DNA does not show any apparent cleavage whereas BNAP and complexes were shown to cleave DNA, it is inferred that these compounds suppress thriving of pathogenic organisms by DNA cleavage. The complexes and BNAP were allowed to transform super coiled DNA into an open round shape. The popular oxidative mechanism occurs due to DNA cleavage by means of hydroxyl radicals through abstraction of H atom from sugar cells and the release of special residues arising from converted sugars depending on the location from which H atom is eliminated[45]. Component that alters DNA cleavage by metal complexes are concentration of complex, character of metal ion, pH of buffer, type of buffer, incubation time, incubation temperature, part of coordinated ligands and addition of H_2O_2 or in presence of ascorbic acid as external reagent[46].The ability of BNAP and complexes to result in DNA cleavage has been explored and shown in **Fig. 13**.

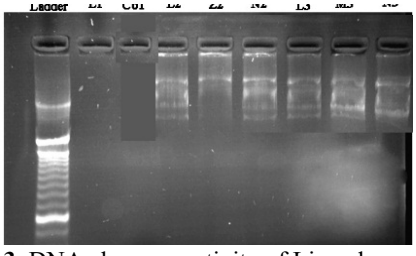

Fig. 13. DNA cleavage activity of Ligands complexes.

It is obvious that BNAP and different metal complexes exhibit different split efficiency for plasmid DNA and it is because of the different binding ability of the complexes to DNA. Control DNA is not showing any apparent cleavage of pUC 18 DNA. The anticancerous study using synthesized Co(II) complex shows activity towards SiHa and SKBR3 at two different concentrations of 0.2 µg/ml and 0.1 µg/ml and control and is shown in **Fig. 14**. The activity of complexes can be attributed to efficiency of DNA binding of complexes because of heteroatoms present in complexes, coordination geometry of complexes and the chelating effect of complexes.

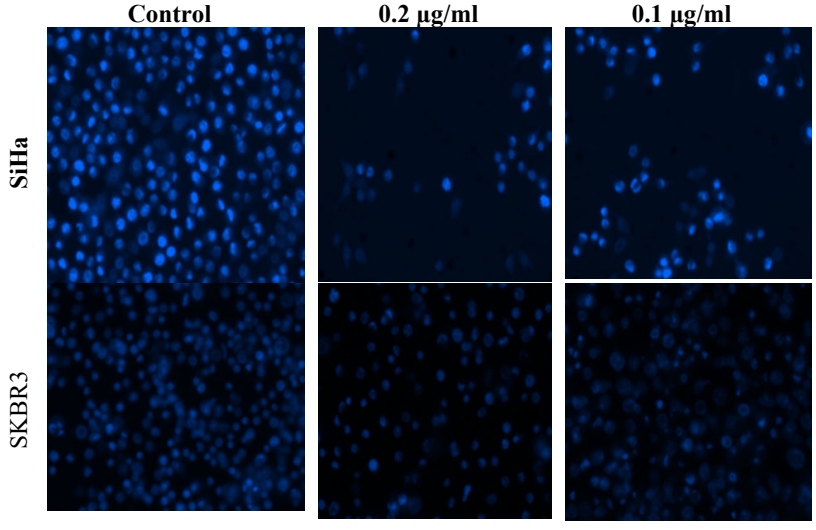

Fig. 14. Image of $[Co(UAAP)(NO_3)_2]$ for SiHa and SKBR3

4. Conclusions

Six new complexes of BNAP with Mn(II), Fe(II), Co(II), Ni(II), Cu(II), Zn(II) and have been prepared and described by elemental analysis, conductance measurements, IR, Mössbauer, electronic spectral studies and magnetic susceptibility measurements. IR spectral evidence declare that BNAP is bidentate uninegative in nature and the presence of coordinated water in complexes. This is more supported by the absence of hydroxyl proton peak in ^{1}HNMR spectra of Zn(II) complex. Molar Conductance values support the non-electrolytic nature of all complexes. Electronic spectra and magnetic moment value holds up octahedral geometry for all except for the Zn(II) complex which has tetrahedral geometry. The stability of the ligand in complexes was confirmed by quasi reversible peak obtained in cyclic voltammetry analysis. None of the ligand and complexes shows non-linear optical properties. The Mn(II) and Ni(II) complexes show enhanced fluorescence. BNAP is found to be more vital against all the studied microbes relative to its complexes. BNAP and its complexes catalysed cleavage of DNA. $[Co(BNAP)_2(H_2O)_2]$ was done, which shows good anticancerous activity. The single crystals of BNAP and complexes, theoretical, docking, catalytic and biomasking properties can be done as scope for future studies.

Acknowledgement

The authors are thankful to RGCB, Trivandrum, for cytotoxic studies, SAIF, CUSAT and Department of Chemistry, University College, Trivandrum for instrumental facilities under DST FIST. The author is thankful to UGC for the FDP support.

Conflicts of interest

The authors do not have any conflict of interest.

References

1. Shankarling, G. S., Deshmukh, P. P. and Joglekar, A. R. (**2017**) Process intensification in azo dyes. *J. Environ. Chem.,* 5, 3302-3308.
2. Gurses, A., Acikyildiz, K. and Gunes, M. S. (**2016**) Classification of dye and pigments. *Dyes Pigm.*, 31-45.
3. Shah, M. (**2018**) Effective treatment systems for azo dye degradation: a joint venture between physic-chemical & microbiological process, *J. Environ. Biorem. Biodegrad*., 2, 974-985.
4. Lipskikh, O. I., Korotkova, E. I., Khristunova, Y. P., Barek, J. and Kratochvil, B. (**2018**) Sensors for voltammetric determination of food azo dyes- a critical review*, Electrochim. Acta*., 20, 974-985.
5. Berradi, M., Hsissou, M., Khudhair, M. Assouag, O., Cherkaoui, A., El Bachiri, A. and El Harfi A. (**2019**) Textile finishing dyes and their impact on aquatic environs. *Heliyon*., 5, 2711.
6. Benkhaya, S. and El Harfi, A. (**2018**) Classification, properties and applications of textile dyes: a review, *Appl. J. Environ. Eng. Sci.,* 3, 1-3.
7. Derkowska-Zienlinska, B., Gondek, E., Pokladko-Kowar, M., Kacz-marek-kedziera, A., Kysil, A., Lakshminarayana, G. and Krupka, O. (**2020**) Photovoltaic cells with various azo dyes as components of the active layer. *Sol. Energy*, 203, 19-24.
8. Derkowska-Zienlinska, B., Matczyszyn, K., Dudek, M., Samoc, M., Czaplicki, R., Kaczmarek-kedziera, A., Smokal, V., Biitseva, A. and Krupka, O. (**2019**) All-optical polling and two-photon absorption in heterocyclic azo dyes with different side groups. *J. Phys. Chem. C.,* 123, 725-734.
9. Derkowska-Zienlinska, B., Szmigiel, D., Kysil, A., Krupka, O., Kaczmarek-kedziera, A. (**2020**) photoresponsive behavior of heterocyclic azo polymers with various functional groups. *J. Phys. Chem. C.,* 124, 939-944.
10. Khalil, A., Aboamera, N. M., Naseer, W. S., Mahmoud,W. H. and Mohammed, G. G., (**2020**) Photo degradation of organic dyes by PAN/SiO_2-TiO_2-NH_2 nanofiber membrane under visible light. Sep. Purif. Technol., 224, 509-514.
11. Wakiel, N. A. (**2016**) Synthesis and characterization of azo sulfaguanidine complexes and their application for corrosion inhibition of silicate glass. *Appl. Organomet. Chem*., 8, 664-673.
12. Raja, P. B., Ismail, M., Ghoreishiamiri, S., Mirza, J., Ismail, M. C., Kakooei, S. and Rahim, A. A. (**2016**) Reviews on corrosion inhibitors: a short review. *Chem. Eng. Commun.,* 203, 1145-1156.
13. Hussain, G., Abass, N., Shabir, G., Athar, M., Saeed, A., Saleem, R., Ali, F. and Khan, M. A. (**2017**) New acid dyes and ther metal complexes based on substituted phenols and optical studies. *J. Appl. Res. Tech.*, 15, 346-355.
14. Gehad, G. M., Walaaa, H. M. and Ahamed, M. R. (**2020**) Nano azoligand and its superhydrophobic complexes: Synthesis, chracterization, DFT, contact angle, molecular docking and antimicrobial studies. *J. Chem*. 2020
15. Alya, M. and Morsy, A. (**2020**) A comprehensive review on the synthesis and versatile applications of biologically active pyridone-based disperse dyes*. Int. J. Env. Res. Pub. He.* 17, 4714.
16. Hatem, E. G. and Tawfik, A. K. (**2017**) Synthesis and characterization of some azo-heterocycles incorporating pyrazalopyridine moeity as disperse dyes. *Egypt. J. Chem*., 2017, 41-47.
17. Myek, B., Batari, M. L., Orijajogum, J. O. and Aboki, M. A. (**2020**) Synthesis and characterization of metal complex of an azo dye based on acid orange 7. *Commun. Phys. Sci*., 5(3), 358-361.
18. Vidya, V. G. and Sadasivan, V. (**2018**) Synthesis, spectral and biological studies of complexes with bidentate azodye ligand derived from resorcinol and 1-amino-2-naphthol-4-sulphonic acid. *Orient. J. of Chem*. 34(1), 44-55.
19. Vogel, A.I. (**1989)** *Text book of Practical Organic Chemistry*, Longman**.**
20. Suman, A. and Nagashri, K., (**2017**) Joseyphus, R. S. and Nisha Balakrishnan. Synthesis, characterization and biological studies of Copper(II) complexes with 2-aminobenzimidazole derivatives*. J. Mol. Struct*., 1137, 17-26.
21. Dilek, C. (**2020**) Synthesis, spectroscopic, thermodynamic and kinetics analysis study of novel polymers containing various azo chromophore. *Sci. Rep.,* 10, 477.
22. Agnieszka, K., Monika, O., Marcin, L., Marcin, S., Tomasz, S. and Rafal, K. (**2020**) 1,3,4-Thiadiazole- containing azo dyes: *Synthesis, spectroscopic properties and molecular structure. Mol*., 25, 2822.
23. Ziyad, T. A., Faiq, F. K., Khalid, A. (**2019**) Synthesis and characterization of some metal complexes with new heterocyclic azo dye ligand 2-[211(5-nitothiazolyi) azo]-4-methyl-5-nitro phenol and their biological activities. *J. Phys.,* 1294.
24. Nakamoto K. (**1978**) Infrared and Raman spectra of inorganic and coordination compounds. New York: Wiley**.**
25. Geary, W. J. (**1971**) The use of conductivity measurements in organic solvents for the characterization of coordination compounds. *Coord. Chem. Rev*, 7: 81-22.

26. Dirk, T., Ana, B. G. and Yann, G. (**2013**) Spin state switching in iron coordination compounds. *Beilstein. J. Org. Chem*., 9, 342-391.
27. Makarim, A. M., Laith. S. J. and Moslam, M. M. (**2021**) Synthesis, spectral and biological studies of Co(III), Ni(II) and Cu(II) complexes with new heterocyclic ligand derived from azo dye. *Sys. Rev. Pharm*., 12(1), 426-434.
28. Lever, A. B. P. (**1984**) Inorganic electronic spectroscopy, Elsevier Publ. Comp., Amsterdam, London, New York., 458-472.
29. Vidya, V. G. and Mini, S. (**2014**) Synthesis, Spectroscopic Characterization and Biological Studies of Copper (II) Complex Derived from Salycyloyl Hydrazide with Furfuraldehyde. *Res. J. Rec. Sci.,* 3,154-156.
30. Vidya V. G. (**2016**) Synthesis, Characterization and Biological Studies of a new Cu(II) Complex Derived from 9-Anthraldehyde and 2-Aminopyridine. *Res. J. Rec. Sci.,* 5(7), 41-43.
31. Basappa, C. Y., Murali, K. and Malathi, C. (**2021**) Bivalent Ni(II), Co(II) and Cu(II) complexes of [(E)- [(2-methyl-1,3-thiazol-5-yl)methylidedne] amino}thiourea: Synthesis, spectral characterization, DNA and invitro anti-bactrerial studies. *Heliyon*, 7(4).
32. Vidya, V. G. and Sadasivan, V. (**2018**) Synthesis and Charaterisation of Metal chelates of (5-(2,3-dimethyl-1-phenyl-3-pyrazolin-5-one-4-ylazo)-^{1}H-pyrimidine-2,4-dione*). Journal of Ultra Chemistry*. 14(2), 57-68.
33. Stephen, S., Claire, W. and Mark, D. (**2017**) Unprecedented inequivalent metal coordination environmets in a mixed ligand dicobalt complex. *Eur. J. Inorg. Chem*.**,** 3707–3713.
34. Hendrik, F., Marrigie, M., C. and Jeanet, C. (**2017**) Cyclic voltammetry data of polypyridine ligands and Co(II)-polyoyridine complexes. *Data Brief.* 22, 436-445.
35. Vidya, V. G. and Sadasivan, V. (**2018**) Synthesis characterization and application of some monoazo dyes derived from various aromatic amines. *Asian J. Chem*., 30(9), 2049-2053.
36. Vidya, V. G.; Meena, S. S. and Sadasivan, V. (**2014**) Synthesis and spectral study of new azo dye and its iron complexes derived from 2-naphthol and 2-amino-3-hydroxypyridine, *AIP Conf. Proc.,* 1620, 622-626.
37. Vidya, V. G. and Sadasivan, V. (**2019**) Synthesis of iron oxide nanoparticles from iron(III) chelates and their characterization. *Int. J. Nanosci.Nanotech*.,15(1), 65-73.
38. Vidya, V. G. Meena, S. S. Sadasivan, V., Mini, S. (**2013**) Spectroscopic studies on Fe(II) and Fe(III) complexes of 5-arylazosubstituted lH-pyrimidine-2,4-dione, *AIP Conf. Proc.,* 1536, 1009-1010.
39. Mini, S., Meena, S. S.; Pramod Bhatt, Sadasivan, V., Vidya, V. G. (**2013**) Synthesis and characterization of Fe (III) complex of an azo dye derived from (2-amino-5-chlorophenyl) phenyl methanone, *AIP Conf. Proc.,* 1536, 1011-1012.
40. Vidya, V. G.; V. Sadasivan.; Mini, S. (**2016**) Zinc Chelates as Activators for Sulphur Vulcanization of Natural Rubber. *Imp. J. Interdisc. Res.,* 10(2), 720-724.
41. Siham, S., Adeline, F., Gerald, L. and Abdelkrim El, (**2019**) Imidazole and Azo-Based Schiff Bases Ligands as Highly Active Antifungal and Antioxidant Components*., Heteroatom Chemistry***,** 2019, 1–8.
42. Israa, N. and Witwit, Z. Y. (**2018**) Synthesis, Characterization, and Biological Efficacy on new mixed ligand complexes based from azo dye of 8-hydroxy quinoline as a primary ligand and imidazole as a secondary ligand with some of transition metal ions, *J. Pharm. Sci. & Res.,* 10(12), 3074-3083.
43. Stefano, P., Simona C., Lucia, S., Rosita, D., Gabriel, T., Carlos, J., Ugo, C. and Pio, I. (**2017**) Synthesis and Antimicrobial Studies of New Antibacterial Azo-Compounds Active against Staphylococcus aureus and Listeria monocytogenes. *Molecules*, 22(8), 1372.
44. Dhanaraj C. J., Ul Hassan I., Johnson, J., Joseph, J. and Selwin Joseyphus, R. (**2016**) Synthesis, spectral characterization, DNA interaction, anticancer and molecular docking studies on some transition metal complexes with bidentate ligand, *J. Photochem. Photobiol. B, Biol.* .162, 115-124.
45. Siham S. and Abbas H. (**2018**) Preparation and Biological Activities of New Heterocyclic Azo Ligand and Some of Its Chelate Complexes. *Nano Biomed. Eng.,* 10(1), 46–55.
46. Al-Adilee, K. and Kyhoiesh, H. A. (**2017**) Preparation and identification of some metal complexes with new heterocyclic azo dye ligand 2-[2-(-1-hydroxy-4-chlorophenyl)azo]-imidazole and their spectral and thermal studies. *J. Mol. Stuct.* 1137, 160-178.